Combust. Sci. Technol., 187: 1110–1138, 2015

ISSN: 0010-2202 print / 1563-521X online
DOI: 10.1080/00102202.2015.1019616

Taylor & Francis
Taylor & Francis Group

EULERIAN–LAGRANGIAN RANS MODEL SIMULATIONS OF THE NIST TURBULENT METHANOL SPRAY FLAME

Shanglong Zhu,[1] Dirk Roekaerts,[2] Artur Pozarlik,[1] and Theo van der Meer[1]

[1]*Laboratory of Thermal Engineering, University of Twente, Enschede, the Netherlands*

[2]*Department of Process and Energy, Delft University of Technology, Delft, the Netherlands*

A methanol spray flame in a combustion chamber of the NIST was simulated using an Eulerian–Lagrangian RANS model. Experimental data and previous numerical investigations by other researchers on this flame were analyzed to develop methods for more comprehensive model validation. The inlet boundary conditions of the spray were generated using semi-empirical models representing atomization, collision, coalescence, and secondary breakup. Experimental information on the trajectory of the spray was used to optimize the parameters of the pressure-swirl atomizer model. The standard k-ε turbulence model was used with enhanced wall treatment. A detailed reaction mechanism of gaseous combustion of methanol was used in the frame of the steady laminar flamelet model. The radiative transfer equations were solved using the discrete ordinates method. In general, the predicted mean velocity components of the gaseous flow and the droplets, the droplet number density, and the Sauter mean diameter (SMD) of the droplets at various heights in the present study show good agreement with the experimental data. Special attention is paid to the relative merits of the employed method to set inlet boundary conditions compared to the alternative method of using a measured droplet size and velocity distribution.

Keywords: Methanol flame; Simulation; Spray combustion; Turbulence

INTRODUCTION

Turbulent spray combustion plays an important role in industrial furnaces, gas turbines, internal combustion engines, oil gasifiers, etc. The combustion efficiency, stability, and pollutant formation strongly depend on the characteristics of the turbulent spray combustion. A better understanding of the fundamental mechanisms together with improved modeling capabilities would help to enhance the efficiency and lead to a cleaner and safer environment (Jenny et al., 2012).

Numerical simulations have been attractive for many years because they provide an easier and safer way to understand the characteristics of combustion in detail compared to experiments. However, the modeling and simulation of the turbulent spray is particularly challenging because complex processes involving turbulence, atomization,

Received 1 May 2013; revised 30 November 2014; accepted 11 February 2015.

Address correspondence to Shanglong Zhu, Laboratory of Thermal Engineering, University of Twente, P.O. Box 217, 7500 AE Enschede, Netherlands. E-mail: zhushanglong@gmail.com

Color versions of one or more of the figures in the article can be found online at www.tandfonline.com/gcst.

evaporation, combustion, and radiative heat transfer are included and they are strongly coupled. To improve the reliability of the spray combustion simulation, it is necessary to validate mathematical models with experimental data.

As described in Jenny et al. (2012), often light fuel oils are used to get a better understanding of the turbulent spray combustion because their properties and reaction mechanisms have been well investigated and are readily available (see, e.g., Düwel et al., 2007; Karpetis and Gomez, 2000; McDonell and Samuelsen, 1995; Widmann and Presser, 2002). The reported experiment carried out by Widmann and Presser (2002) at the National Institute of Standards and Technology (NIST) led to the creation of a database of a methanol spray flame (NIST, 2010). As reported in Presser (2006), the predicted spray characteristics are sensitive to the model representation of the spray inlet boundary conditions. Compared to other flames, a relative advantage of the NIST flame is that a lot of attention was paid to accurate measurement of the droplet size and velocity distributions close to the injector in order to provide good boundary conditions for the simulation. Three gas velocity components were obtained from the particle image velocimetry (PIV) measurements at three heights within the chamber for the cases with non-burning and with burning spray (cold and hot states). Droplet size distributions, Sauter mean diameter (SMD), droplet mean axial and radial velocities, and droplet number density were measured at various axial locations downstream of the nozzle exit. The combination of accurate boundary conditions and relatively large amounts of data make this database very valuable for validation.

Several research groups (Collazo et al., 2009; Crocker et al., 2001; De Jager, 2008) have used this database for the validation of their simulations. Their modeling approaches are all based on Reynolds-averaged Navier–Stokes equations (RANS), since large eddy simulation (LES) and direct numerical simulation (DNS) are computationally too expensive due to their high spatial and temporal resolution requirements for this flame. Crocker et al. (2001) and Collazo et al. (2009) carried out Eulerian–Lagrangian RANS simulations while De Jager (2008) employed an Eulerian–Eulerian RANS simulation. Some agreements with the experiment were found in their simulation results. However, as it will be discussed in the following section, either only a limited part of this database was used for validation or boundary conditions of the NIST flame were not analyzed in detail. We will follow the line of modeling with RANS simulations and simulate the NIST flame based on the analysis of boundary conditions and the above mentioned numerical studies in order to handle accurately important aspects of turbulence modulation, evaporation, mixing, and detailed chemistry. Additionally, the advantages of such a way of spray modeling are illustrated and the sensitivities of influential parameters in the spray model are discussed.

EXPERIMENTAL DATABASE

Experiment

The NIST flame experiment was carried out in a combustion chamber, which is shown in the drawing of Figure 1. The chamber height is 1.2 m and the inner diameter is 0.8 m. The flame is fired vertically upwards. The exhaust channel is off-axis to permit direct probing of the flame from above. Swirling combustion air generated by a movable 12-vane swirl cascade passes through the outer annulus passage, with a flow rate of 0.01575 ± 0.0005 m^3/s at ambient pressure and temperature. The inner and outer diameters of the annulus are 34.9 mm and 101.6 mm, respectively. A pressure-jet nozzle forms a hollow-cone methanol spray with a nominal 60° full cone angle at ambient temperature and it is surrounded by the annulus passage. The nominal upstream pressure of the liquid fed to the nozzle is

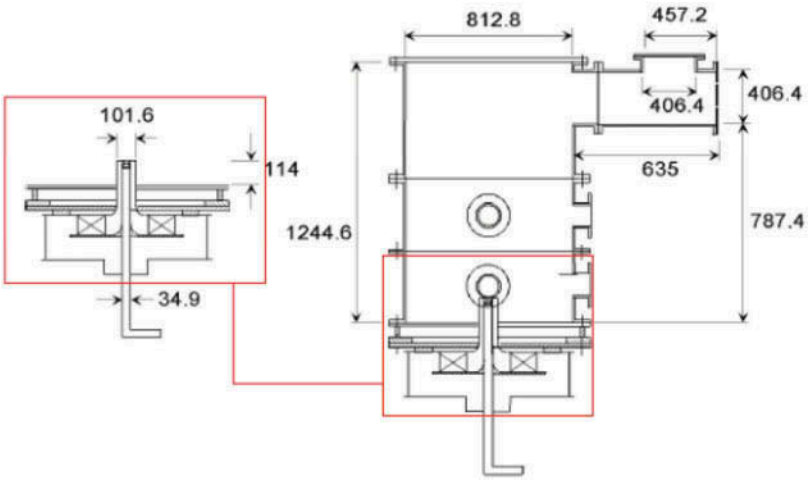

Figure 1 Sketch and dimensions (mm) of the NIST reference spray combustor.

maintained at 690 kPa and the flow rate is kept at 0.00083 ± 0.000006 kg/s. More details regarding the set-up of the configuration can be found in the work of Widmann and Presser (2002).

By using a PIV system, the gas phase axial, radial, and tangential velocities at various heights (1.4 mm, 9.5 mm, and 17.6 mm from the nozzle exit) were measured. The axial and radial particle velocities and the diameter of the droplets were obtained using a phase Doppler interferometer (PDI) along the cross section at seven heights in the range from 5 mm to 65 mm. Sheathed K-type thermocouples were used to measure the wall temperatures at various elevations and gas temperatures at the exit. Concentrations of CO_2, CH_3OH, and CO were measured at the exit of the exhaust channel. No minor components or reaction intermediates were identified. More details are available in NIST (2010).

Previous Modeling

As mentioned above, several investigations of the NIST flame have been made before. In order to obtain a better understanding of the NIST flame and the corresponding simulation aspects, it is necessary to review and analyze the previous simulations, and the predictions in the present study will be discussed and compared in relation to previous results.

With a two-dimensional (2D) axisymmetric Eulerian–Lagrangian RANS simulation using CFD-ACE, Crocker et al. (2001) computed the NIST flame for both non-reacting and reacting cases. The RNG k–ε model was used for turbulent gas flow, and combustion was modeled using a one-step, finite-rate reaction with equilibrium products of CO_2, H_2O, CO, H_2, OH, and O, proposed by Westbrook and Dryer. The measured velocity profiles at height $z = 1.4$ mm in the cold state were assumed to be the initial conditions of the inlet air, and the measured droplet diameter and velocity components of the droplets at height z = 5 mm were analyzed for obtaining the initial boundary conditions of the spray in the simulation. The fuel oil was then assumed to be injected at height $z = 5$ mm as droplet parcels at 30 radial locations, with 20 different droplet sizes, 5 different velocity magnitudes, and 7 different angles (directions) at each radial location. The spray volume flux, spray velocity

components, and droplet SMD were compared with the experimental data, and they showed good agreement. However, due to the very low measured spray flux in the near-nozzle region, the measured data of droplets at height $z = 5$ mm was considered to be insufficient to describe the initial conditions of the droplets. Data of the droplets were further modified to some specific values in the simulation in order to fit one subset of the measured data while other subsets were found to be difficult to fit. Since the droplets were injected from height $z = 5$ mm in the investigation of Crocker et al. (2001), the secondary break-up process was not included. Predictions of velocity components of the gaseous phase were not compared with the experimental data in detail and the evaporation process of the droplets was not discussed either. An aspect worthy to note is that, as a result of the estimation of the spray trajectories for the initial boundary condition of the spray, the predicted spray velocity components and SMD of droplets with low number densities showed good agreement with measured data. It will be discussed and compared with the predictions from the present study later.

De Jager (2008) employed an Eulerian–Eulerian approach and introduced a CFI model for the composition of the gaseous phase, in which C, F, and I represent a reaction progress variable, the mixing scalar, and enthalpy scalar, respectively. The fluctuations are described by a β-PDF for C and F, and the δ-PDF for the normalized enthalpy loss I. The predicted velocity components of the combustion air at heights $z = 9.5$ mm and $z = 17.6$ mm were compared with the experimental data at both non-burning and burning conditions. Significant discrepancies of radial and tangential velocities of the gaseous phase between simulation and experiment were found. The author indicated that turbulence is modeled poorly using the k-ε model, and the proposed spray model in its current form with the Eulerian–Eulerian approach is limited and needs further improvement. The interaction between spray and combustion air needs more attention, especially in the near nozzle region. The suggestion was given by the author that it would be beneficial to implement spray effects in simulations with a Lagrangian description of the droplets, to represent the effects of coalescence and secondary break-up, to reach a more accurate prediction of the SMD.

Collazo et al. (2009) presented results of Eulerian–Lagrangian RANS simulations with a 3D geometry. The interaction processes between droplets and continuous phase were simulated by use of the dispersed phase model, and the linearized instability sheet atomization (LISA) model of Schmidt et al. (1999b). The standard k-ε model was used to simulate the turbulence. For combustion, the eddy dissipation concept (EDC) model proposed by Magnussen (1981) was applied with a two-step reaction of methanol with oxygen, including carbon monoxide. Predictions of droplet diameters, droplet trajectories, temperatures, and gas concentrations were presented and compared with the NIST database (see Widmann and Presser, 2002). The prediction of droplet properties showed some discrepancies, and the authors deduced that the initial spray angle should be higher than 60°. Temperatures and carbon dioxide concentration at the exhaust of the system were well predicted in the simulation of Collazo et al. (2009), while the peak temperature of the flame was overestimated and the concentration of intermediate species was relatively inaccurate. Since neither the results of the velocities of air or droplets were presented, the turbulence model was not validated in this paper.

In both simulations of De Jager (2008) and Collazo et al. (2009), the SMD of the droplets and the droplet number density at various heights were compared with the experimental data. However, their results from the simulations were all studied under cold state without combustion while the reported spray measurements were conducted in the reacting

flow in the experiment. This was confirmed in a private communication by Presser (one of the authors of the NIST experiment; see Widmann and Presser, 2002). In the present study, simulation of the NIST flame and its validation is done for both gaseous phase and spray, based on the analysis of features of the burning flame and experience obtained from previous simulations.

Methods of the Present Study

Based on the analysis of previous simulations of the NIST flame, in the present study, an Eulerian–Lagrangian RANS approach with modeling of droplet collision and secondary break-up is used to obtain an improved prediction of the spray in ANSYS Fluent. The exhaust channel is omitted in the simulation since it is shown in Crocker et al. (2001) that it has little influence on the simulation in the near-nozzle region. The measured velocity components of the gaseous phase at height $z = 1.4$ mm under hot state are used for the boundary condition of the inlet air ($z = 0$ mm), and the corresponding predicted velocity components of the gaseous phase at height $z = 1.4$ mm are compared with the measured data to test the validity of this method. Attention is paid to the analysis of the spray trajectories in order to obtain an accurate boundary condition of the spray. The numerical simulation is performed with the steady laminar flamelet model in order to include detailed chemistry, and the influence of the evaporation on mixture fraction variance is investigated. Predictions of the mean velocity components of air flow and droplets, droplet number density, and SMD is compared with the experimental data and previous predictions mentioned above in order to get a better understanding of this turbulent spray flame.

MATHEMATICAL MODELS

Computational Domain, Grid, and Turbulence Model

For the simulation of the NIST flame, as we discussed above, the influence of the exhaust channel on the simulation of the near-nozzle region is negligible and it can be omitted in the geometry, considering the end of the combustion chamber as an open boundary. As a result, the 2D axisymmetric simulation with swirl is employed in the present study.

The grid independence was tested by introducing a series of different cell sizes with the same axial/radial aspect ratio of 3. The role of the near-wall treatment for this swirling flow was analyzed. As a result, a 2D mesh with about 46,000 quadrilateral cells (as shown in Figure 2) in combination with the second-order upwind scheme was found suitable for this study. A standard k-ε turbulence model with the enhanced wall treatment is employed based on the comparative analysis. The use of the enhanced wall treatment can possess the accuracy of the standard two-layer (a viscosity affected region and a fully-turbulent region) approach for fine near-wall mesh and at the same time, not to reduce accuracy for the wall-function mesh. Its application is dependent on both the grid and flow characteristics, and we found that this is of particular significance for the prediction of the profile of radial velocity of the gaseous phase.

Spray Model

Model for droplet diameter distribution. The atomization process of light oil sprays is commonly modeled using a wave growth or aerodynamic theory that predicts

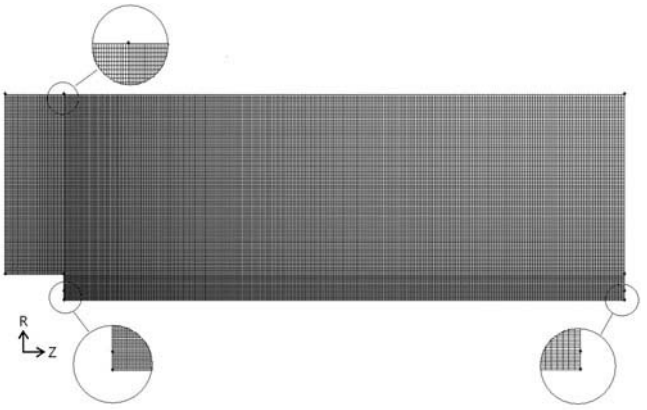

Figure 2 2D mesh with about 46,000 quadrilateral cells.

spray parameters, such as the spray angle and the drop diameter. The surface wave instability model proposed by Reitz (1987), the Kelvin–Helmholtz/Rayleigh–Taylor (KHRT) instability model by Patterson and Reitz (1998), and the Taylor analogy breakup (TAB) model by O'Rourke and Amsden (1987) are widely used atomization models. However, their coupling with the nozzle effects and the primary breakup is largely unknown and is usually represented by an arbitrary nozzle-dependent constant.

For the pressure swirl atomizer in the NIST flame, we employ the LISA model as presented by Schmidt et al. (1999a). It assumes that Kelvin–Helmholtz waves grow on the sheet and eventually break the liquid into ligaments. It is then assumed that the ligaments break up into droplets due to varicose instability. Once the liquid droplets are formed, the spray evolution is determined by drag, collision, coalescence, and secondary breakup.

For film formation, the relationship between the thickness of this film, t, and the mass flow rate is as follows:

$$\dot{m}_{eff} = \pi \rho u t (d_{inj} - t) \tag{1}$$

where d_{inj} is the injector exit diameter, $\dot{m}_{eff}$ is the effective mass flow rate, and u is the mean axial component of velocity at the injector exit. Because u depends on internal details of the injector and is difficult to calculate from first principles, the approach of Han et al. (1997) is used and the velocity magnitude is assumed to be related to the injector pressure by:

$$U = k_v \sqrt{\frac{2\Delta P}{\rho_l}} \tag{2}$$

where k_v is a dimensionless velocity coefficient and a function of the injector design and injection pressure (see, for details, Lefebvre, 1989). If ΔP is known, u can be calculated as:

$$u = U \cos\theta \tag{3}$$

where θ is the spray angle.

The pressure-swirl atomizer model for sheet breakup and atomization includes the effects of the surrounding gas, liquid viscosity, and surface tension on the breakup of the liquid sheet. It is based upon the growth of sinusoidal waves on the liquid sheet. For waves that are long compared with the sheet thickness, ligaments are assumed to be formed from the sheet breakup process once the unstable waves reach a critical amplitude. If the surface disturbance has reached a value of η_b at a breakup time τ, the sheet breaks up and ligaments will be formed at a length given by:

$$L_b = U_\tau = \frac{U}{\Omega} \ln\left(\frac{\eta_b}{\eta_O}\right) \tag{4}$$

where Ω is the maximum growth rate, and $\ln\left(\eta_b/\eta_O\right)$ is an empirical sheet constant for which a default value of 12 was obtained theoretically by Weber (1931) for liquid jets. Dombrowski and Hooper (1962) also showed that a value of 12 for the sheet constant agreed favorably with experimental sheet breakup lengths over a range of Weber numbers from 2 to 200.

Thus, the diameter of the ligaments formed at the point of breakup can be obtained from a mass balance. If it is assumed that the ligaments are formed from tears in the sheet twice per wavelength, the resulting diameter is given by:

$$d_L = \sqrt{\frac{8h}{K_S}} \tag{5}$$

where K_S is the wave number corresponding to the maximum growth rate, and the film thickness can be calculated from the breakup length and the radial distance from the center line to the mid-line of the sheet at the atomizer exit r_0:

$$h_{end} = \frac{r_0 h_0}{r_0 + L_b \sin\left(\frac{\theta}{2}\right)} \tag{6}$$

For waves that are short compared to the sheet thickness, this mechanism is not used. The ligament diameter is assumed to be linearly proportional to the wavelength that breaks up the sheet:

$$d_L = \frac{2\pi C_L}{K_S} \tag{7}$$

where C_L is the ligament constant equal to 0.5 by default.

In either the long-wave or the short-wave case, the breakup from ligaments to droplets is assumed to behave according to Weber's analysis for capillary instability (Weber, 1931). So the most probable diameter for droplet diameter distribution, d_0, is determined from:

$$d_0 = 1.88 d_L (1 + 3Oh)^{1/6} \tag{8}$$

where Oh is the Ohnesorge number, which is a combination of the Reynolds number and the Weber number.

Once this most probable droplet size for a Rosin–Rammler distribution has been determined, with a spread parameter and a dispersion angle, which are equal to 3.5° and 6° based on past modeling experience of Schmidt (1999), respectively, the droplet diameter distribution is determined.

Model for spray evolution. In the simulation, the fuel is assumed to be injected into the chamber as a fully atomized spray consisting of spherical droplets of various sizes. The motions of the droplets in the turbulent combustion flow field are calculated using a stochastic method in which the momentum, mass, and energy exchange between the droplets and the gas phase is simulated while tracking a large number of droplets.

The equation of motion for a droplet is:

$$\frac{du_{p,i}}{dt} = \frac{18\mu}{\rho_p D_p^2}\frac{C_D \mathrm{Re}}{24}\left(U_i - u_{p,i}\right) + \frac{g_i\left(\rho_p - \rho\right)}{\rho_P} + F_i \tag{9}$$

In this equation, $u_{p,i}$ is the velocity of droplet (particle) i, U is a sampled gas velocity, μ is the molecular viscosity of the fluid, ρ is the fluid density, ρ_p is the density of the particle, D_p is the particle diameter, Re is the relative Reynolds number based on slip velocity and particle diameter, and the drag coefficient C_D is a function of the particle Reynolds number. F_i is a possible additional acceleration term. In practice, a number of 'parcels', each representing a set of identical droplets, is tracked.

For secondary breakup, the TAB model, which is based upon Taylor's analogy, as described in Taylor (1963), between an oscillating and distorting droplet and a spring mass system, is employed since the investigated case has relatively low Weber number injections (Weber number less than 100) and the TAB model is well suited for low-speed sprays into a standard atmosphere (see Dombrowski and Hooper, 1962).

For droplet collision and coalescence, the algorithm of O'Rourke (1981) is employed. It uses the concept of a collision volume to calculate the probability of collision. In general, once two parcels are supposed to collide, the outcome tends to be coalescence if they collide head-on, and bouncing if the collision is more oblique. The probability of coalescence can be related to the offset of the collector droplet center and the trajectory of the smaller droplet. The critical offset is a function of the collisional Weber number and the relative radii of the collector and the smaller droplet.

The rate of vaporization is governed by gradient diffusion, with the flux of droplet vapor into the gas phase related to the difference in vapor concentration at the droplet surface and the bulk gas:

$$N_i = k_c\left(C_{i,s} - C_{i,\infty}\right) \tag{10}$$

where N_i is the molar flux of vapor, $C_{i,s}$ is the vapor concentration at the droplet surface, and $C_{i,\infty}$ is the vapor concentration in the bulk gas. k_c is the mass transfer coefficient calculated from the Sherwood number correlation (see Ranz and Marshall, 1952a, 1952b), and is defined as:

$$Sh_{AB} = \frac{k_c D_p}{D_{i,m}} = 2.0 + 0.6\mathrm{Re}^{1/2} Sc^{1/3} \tag{11}$$

where $D_{i,m}$ is the diffusion coefficient of vapor in the bulk and Sc is the Schmidt number. The concentration of vapor at the droplet surface is evaluated by assuming that the partial

pressure of vapor at the interface is equal to the saturated vapor pressure, p_{sat}, at the droplet temperature, T_p:

$$C_{i,s} = \frac{p_{sat}(T_p)}{RT_p} \tag{12}$$

where R is the universal gas constant.

Radiation and Combustion Model

By comparison of the predictions with and without the radiation model, it was found that radiative heat transfer cannot be neglected in the simulation of the NIST flame. The difference of the peak temperature can be as high as about 200 K. Therefore, in this study, the discrete ordinates (DO) radiation model with a variable absorption coefficient, weighted-sum-of-gray-gases model (WSGGM) is employed.

As a combustion model, a one-step global reaction mechanism with the eddy dissipation model (ED) is often used in spray combustion simulations. However, this model often leads to overestimated temperature predictions, and sometimes detailed chemistry is also necessary for the prediction of ignition and extinction processes, as well as the pollutant formation. According to the relative fast chemistry of methanol, the laminar flamelet method provides a feasible way here to include detailed chemical reactions in turbulent combustion simulations without a considerable increase in computational time. It assumes that in the gaseous phase combustion, the diffusion coefficients for all species are equal, and then the species mass fraction and temperature are mapped from physical space to mixture fraction space and can be uniquely described by two parameters: the mixture fraction, ξ, and the scalar dissipation, χ. Figure 3 shows results contained in the look-up table. The Favre-averaged values of quantities in the turbulent flame are then obtained through the use of Favre-averaged probability density function, $\tilde{f}(\xi, \chi)$:

$$\tilde{\Phi} = \int_0^\infty \int_0^1 \Phi(\xi, \chi)\tilde{f}(\xi, \chi)\, d\xi\, d\chi \tag{13}$$

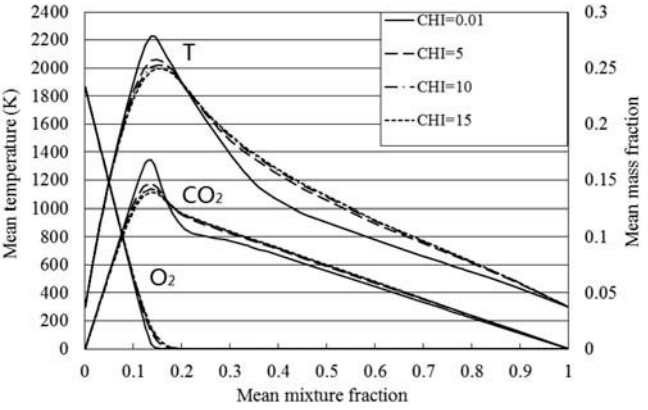

Figure 3 Steady flamelet profiles stored in the look-up table (CHI $\equiv \tilde{\chi}$ [s^{-1}]).

The detailed reaction mechanism for methanol employed in the present study was developed by Lindstedt and Meyer (2002) and provided by Lindstedt and Chen (2010) with a Chemkin compatible reduced mechanism. It comprises 32 species and 167 reactions.

In the model, the heat gain/loss to the system is assumed to have a negligible effect on the species mass fractions, and adiabatic mass fractions are used (see also Muller et al, 1994; Binniger et al., 1998). The flamelet profiles are then convoluted with the assumed β-function-shape PDFs as in Eq. (13), and then tabulated for look-up. The equations for the mean mixture fraction, mixture fraction variance, and mean enthalpy are solved. The scalar dissipation field is calculated from the turbulence fields $\tilde{k}$, $\tilde{\varepsilon}$, and the mixture fraction variance $\tilde{\xi}''^2$ as follows:

$$\tilde{\chi} = \frac{C_\chi \tilde{\varepsilon} \tilde{\xi}''^2}{\tilde{k}} \tag{14}$$

where C_χ is set to the standard value 2.

The mean values of temperature, density, and species mass fraction are obtained from the PDF look-up table.

Furthermore, in order to investigate the influence of a source term, $\bar{\dot{\rho}}_s \tilde{\xi}''^2 (1 - 2\tilde{\xi})\tilde{\xi}$ due to evaporation in the mixture fraction variance equation (see Hollmann and Gutheil, 1996), calculations were made with and without this source term included.

Boundary Conditions

An accurate representation of the boundary conditions is essential to carrying out a successful simulation, as discussed in Presser (2006). With respect to the air inlet conditions, the mass flow and the temperature for the simulation are shown in Table 1. The air velocity components at height $z = 1.4$ mm near the air inlet, both with and without the spray, are measured in the experiment. Based on the previous simulations and analysis, the velocity components at this elevation can represent the inlet conditions, and the data measured when the spray flame is present are supposed to be a better assumption for the simulation of the spray combustion. This will be discussed in the next section.

With regard to the spray, the mass flow rate, temperature of methanol, the injector pressure, and spray angle for the simulation based on the experiment are shown in Table 1. However, the injector exit diameter, d_{inj}, in Eq. (1) and the parameters for the droplet diameter distribution in the LISA model are not well defined, and we have to deduce them from the experimental data in order to obtain a relative accurate spray trajectory.

The droplet number density at seven axial locations downstream of the nozzle exit (z = 5, 15, 25, 35, 45, 55, and 65 mm) from the experiment of Widmann and Presser (2002)

Table 1 Inlet conditions of air and fuel

Air flow rate (m^3/h)	~56.7[a]
Air temperature (K)	298
Fuel flow rate (kg/h)	3.0
Fuel temperature (K)	298
Injection pressure (Pa)	690,000
Spray angle (°)	60

[a]Interpolated data within 5% relative error.

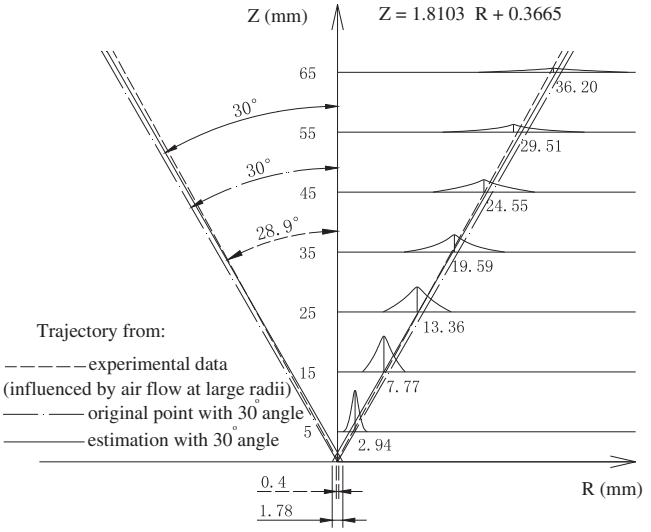

Figure 4 Estimation of the spreading angle of the spray.

was analyzed to estimate the injector exit diameter, as shown in Figure 4. The short dashed line represents the trajectory obtained in the experiment by linking the location of the peak number density at each elevation. The long dashed line represents the trajectory from the point of origin with the spray angle of 60°. As we can see from Figure 4, at large radii, the trajectory of the spray in the experiment is already influenced by the co-flow and thus the spray angle is less than 60°. Therefore, to estimate the initial trajectory of the spray, we kept the spray angle of 60° and used the data of locations where the spray is less influenced by the co-flow.

As a result, the trajectory of the spray was estimated, as shown in Figure 4, with the solid line. The injector exit diameter in Eq. (1) is then set to be 1.78 mm. The sensitivity of this parameter on the predictions is discussed in the following section. Furthermore, the influence of the dispersion angle, sheet constant, and ligament constant on the predicted results were investigated as well. The effect of dispersion angle on droplet size distribution and temperature profiles is shown in the following section. A combination of a dispersion angle of 10°, a sheet constant of 12, and a ligament constant of 0.5 was employed in our simulations.

For the walls, a convection coefficient with the ambient air of 12 Wm^{-2} K^{-1} and a surrounding temperature of 298 K (also used in work of Collazo et al. (2009)) were adopted.

RESULTS AND DISCUSSION

Numerical and experimental data of air mean velocity components at height $z =$ 1.4 mm are presented in Figure 5. The uncertainty of the experimental measurements is represented by error bars. The experimental data at this height were measured from radius 19.6 mm to 50.0 mm with a PIV system. Since PIV measurement at lower heights in the near-field region of the nozzle is not possible, data at height $z = 1.4$ mm are used as numerical inlet boundary conditions at height $z = 0$ mm for the combustion air flow. The corresponding computational predictions of air flow mean velocity components at height

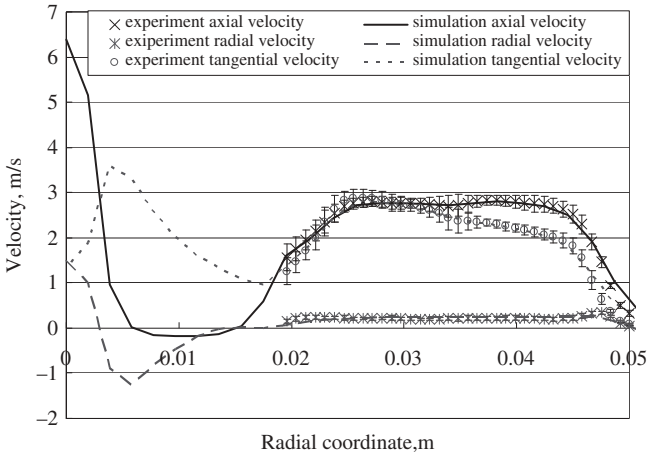

Figure 5 Predicted mean velocity components at $z = 1.4$ mm compared with experiment.

$z = 1.4$ mm are compared with the measured data at the same location in Figure 5. It can be noted that numerical and experimental data are very close to each other in the measured region. No high gradient velocity is observed due to either flue gas entrainment or radiation from the flame, suggesting that the measured velocity components at height $z = 1.4$ mm at hot state are accurate enough to be used as inlet boundary conditions for the combustion air.

Figures 6 and 7 show the computed mean gas velocity components at heights $z = 9.5$ mm and $z = 17.6$ mm, respectively. These data are compared with predictions of De Jager (2008) and the experiment of Widmann and Presser (2002). At large radii (above 30 mm), where the flow field is dominated not by the spray but by the air flow, the present study shows good agreement with experimental data for mean gas velocity components. The deviations at large radii for the tangential velocity at $z = 9.5$ mm and $z = 17.6$ mm seem to be remarkable. However, superimposing the influence of the measurement errors of the data at $z = 1.4$ mm shown in Figure 5, which affects the inlet conditions, the deviations are still minor. For radii below 30 mm (in particular for radii smaller than the inner radius of the combustion air inlet, i.e., 17.45 mm), major deviations from the experimental data for axial and radial velocities can be observed. This is also visible in the work of De Jager (2008). This flow behavior can be an effect of an overestimation of the interaction between the droplets and the continuous phase. However, because the acceleration of the continuous phase by the spray and thermal expansion of the continuous phase should result in enhanced velocity components, an alternative more probable explanation can be found, i.e., although velocity components of the gaseous phase are accelerated by the spray, it is difficult to measure them in a region where a dispersed phase is present in high concentration (along the droplet trajectory) due to the similar scattering feature of droplets as the induced particles during measurement. For the tangential velocity, the predicted results at small radii resemble the experimental data well because the tangential velocity is less influenced by the spray.

Due to the assumptions of pre-evaporated fuel used in the simulation of De Jager (2008), the predicted axial velocity profile observed in his results has a peak value of

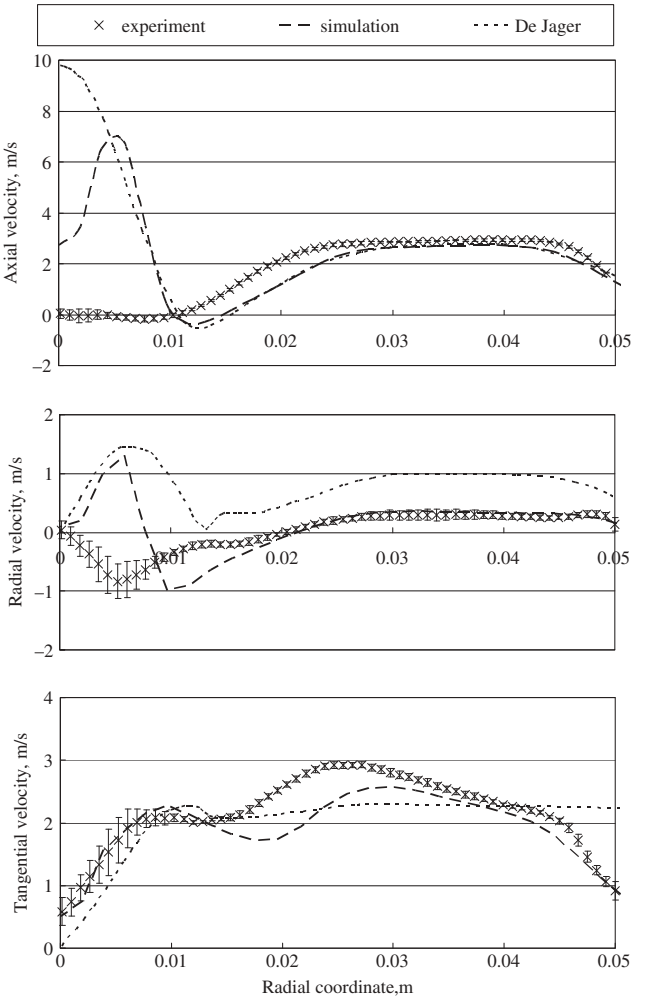

Figure 6 Predicted mean velocity components at $z = 9.5$ mm compared with De Jager's results and the experiment.

9.7 m/s at the central line ($z = 9.5$ mm). In the present study, a peak value of 6.9 m/s occurs at a radial position about 5 mm away from the central line, which means the gaseous phase is dragged by the spray along the injection trajectory. This is also observed in the simulation results of Crocker et al. (2001) with a narrow region of accelerated flow near the nozzle tip caused by liquid spray entrainment. Large discrepancies between predicted radial and tangential velocities from De Jager (2008) computation and the experimental data can be observed. That is most likely attributed to the near-wall treatment introduced in the turbulence model. In this case, the heights at which data were measured are close to the nozzle, and the influence of the tip of the atomizer needs to be taken into account. According to the $y+$ value in the near-wall region, a more accurate prediction can be obtained by using the enhanced wall treatment (Kader, 1981), instead of the wall function used by De Jager (2008).

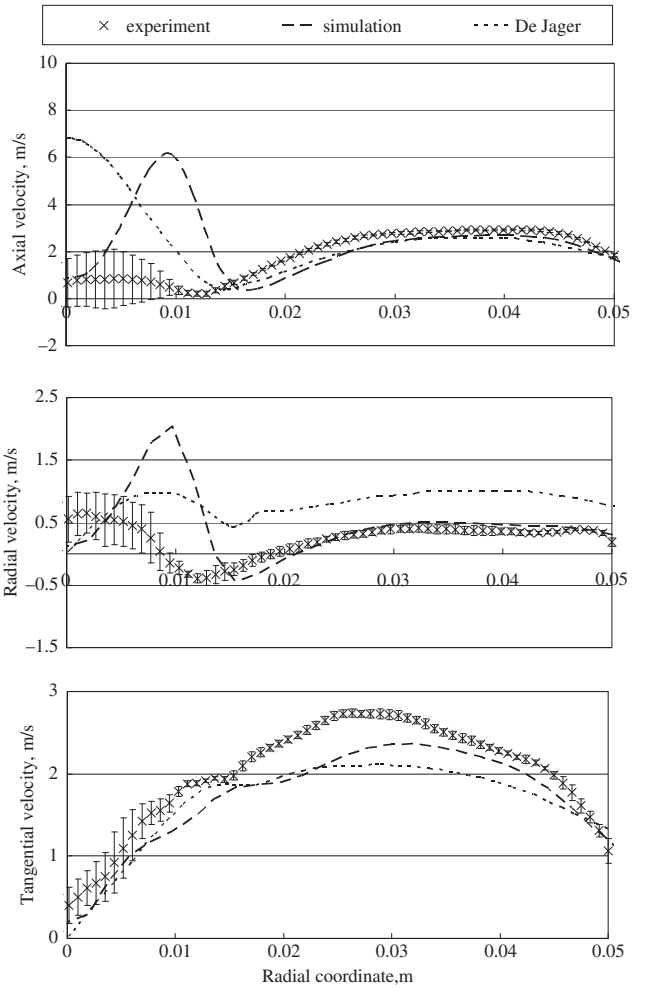

Figure 7 Predicted mean velocity components at $z = 17.6$ mm compared with De Jager's results and the experiment.

Figure 8a shows the spray volume flux at different heights from the simulation of Crocker et al. (2001) compared with the experiment of Widmann and Presser (2002). The magnitude of the peak at height $z = 15$ mm is predicted to be significantly higher than the experimental data. This phenomenon is also observed in the present study (see Figure 8b for comparison of droplet number density between numerical and experimental data) At further downstream locations, i.e., heights $z = 35$ mm and $z = 55$ mm, peak magnitudes of spray volume fluxes from the simulation of Crocker et al. (2001) occur at different radial locations from the experimental. Therefore, it was proposed by the authors to increase all of the initial spray angles by 3° in order to better evaluate the sensitivity of the spray flux location to the initial spray angle. Since the predicted droplet velocity and SMD in the work of Crocker et al. (2001) shows good agreement with the experiment without adjustment of initial spray angles, this modification may entail more significant discrepancy in both profiles because the spray trajectory differs significantly with a 3° change. In the present

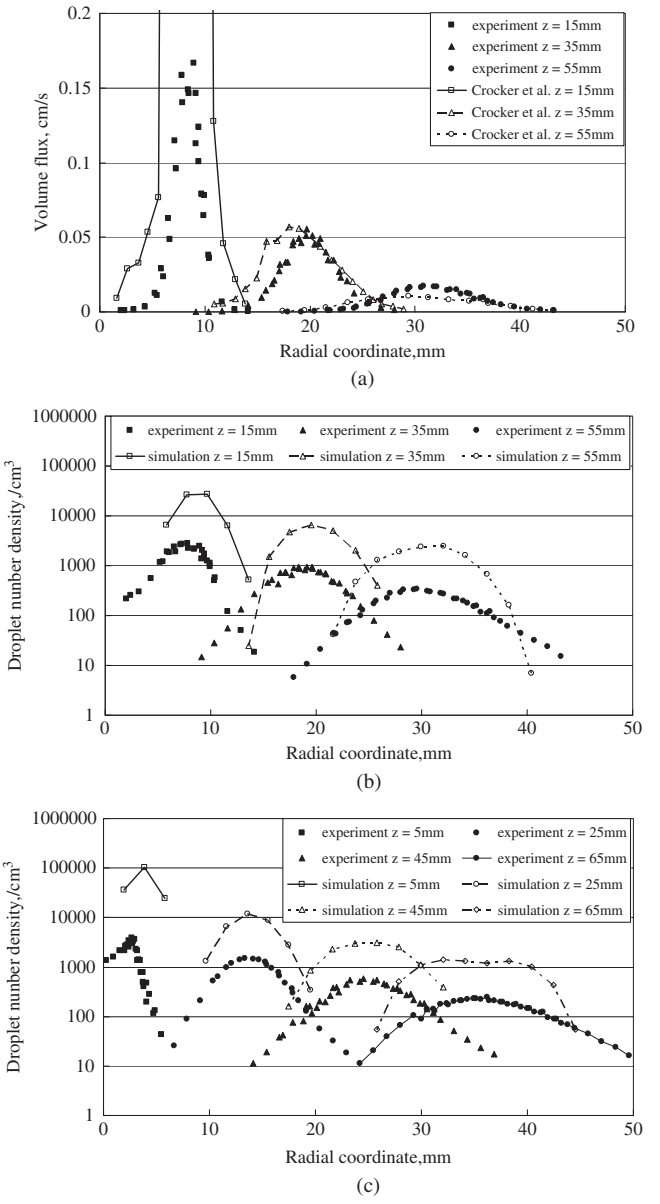

Figure 8 Predicted spray volume flux/droplet number density at different heights compared with results from Crocker et al. (2001) and the experiment.

study, an increased dispersion angle of 10° is introduced instead of the initial spray angle, resulting in the peak positions and trends all being in good agreement with the experimental data. This behavior is observed not only at $z = 15$ mm, 35 mm, and 55 mm heights, but also at four other elevations shown in Figure 8c. The main difference here is that the simulation of the present study provides higher droplet number density than the experiment. Closer to the atomizer, at lower heights, the predicted number of droplets increases leading

to major overestimation of the experimental data. This is reasonable because accurate measurements of droplet number density in the high number density region close to the nozzle are very difficult. During measurement only a small portion of droplets can be captured and quantified. That is why it has been suggested by Widmann, and Presser (2002) to use the information about the droplet number density in a qualitative way rather than quantitatively. Also, in the work of Crocker et al. (2001) this large difference of droplet number density is also observed at a height of mm. From Figure 8a, it can be concluded that at a height of 35 mm a similar number of droplets was observed in computations as in experiments; however, at a height of 55 mm more droplets were captured in the experiment than by the simulation. The present study shows that there are always less droplets observed during measurement than are recorded by the simulation; also by approaching the nozzle progressively, fewer droplets are being observed. Figure 9 depicts the predicted droplet number

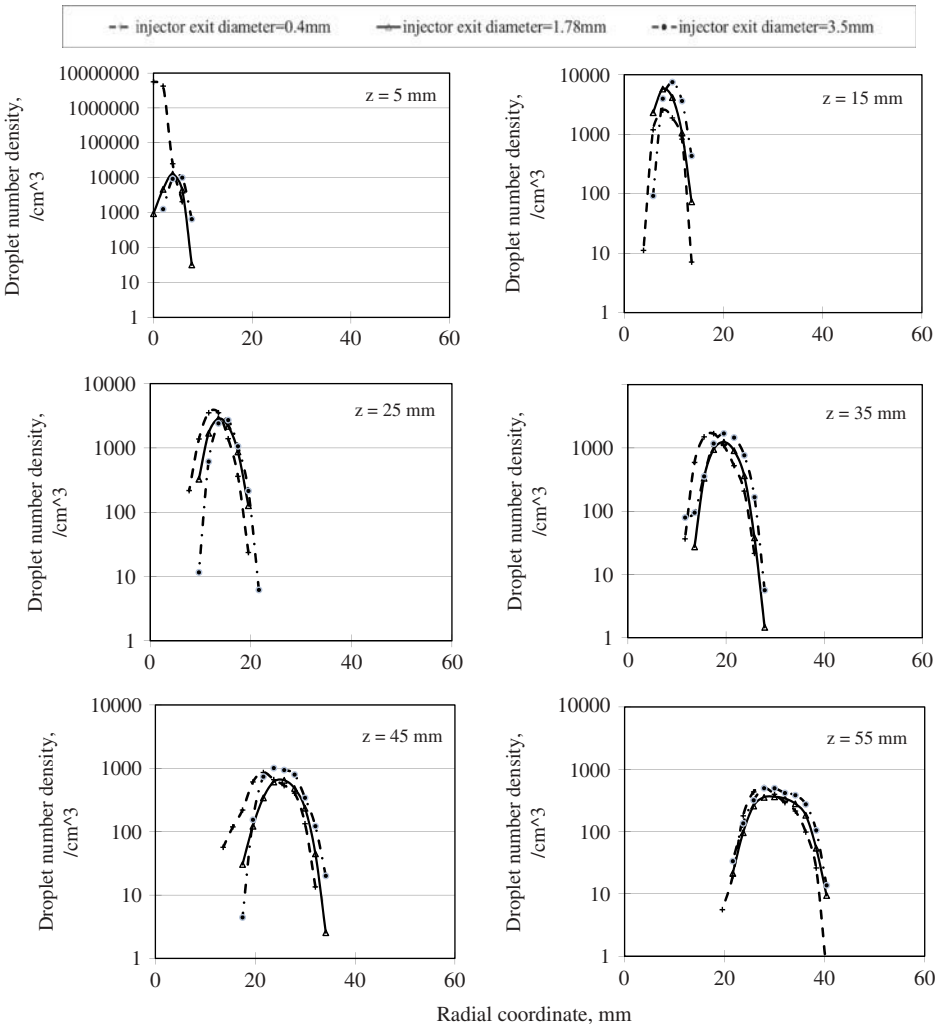

Figure 9 Predicted droplet number density at different heights with different injector exit diameters.

density at various heights with different injector exit diameters. All injections are pointing outwards. With a small injector exit diameter of 0.4 mm, the droplet number density at $z =$ 5 mm is much higher than for the 1.78 mm and 3.5 mm and approaches the centerline of the nozzle. Since the mass flow of the fuel is constant, this indicates that a considerable amount of small droplets is generated. The behavior like that is also observed at the same height in Figure 10, which represents the predicted Sauter mean diameter for various injector exit diameters. The small droplets evaporate very quickly leading to the droplet number density at height $z = 15$ mm, which is even lower than for the other two cases. The region on the left-hand side of the peak in droplet number density is a region confined by the spray,

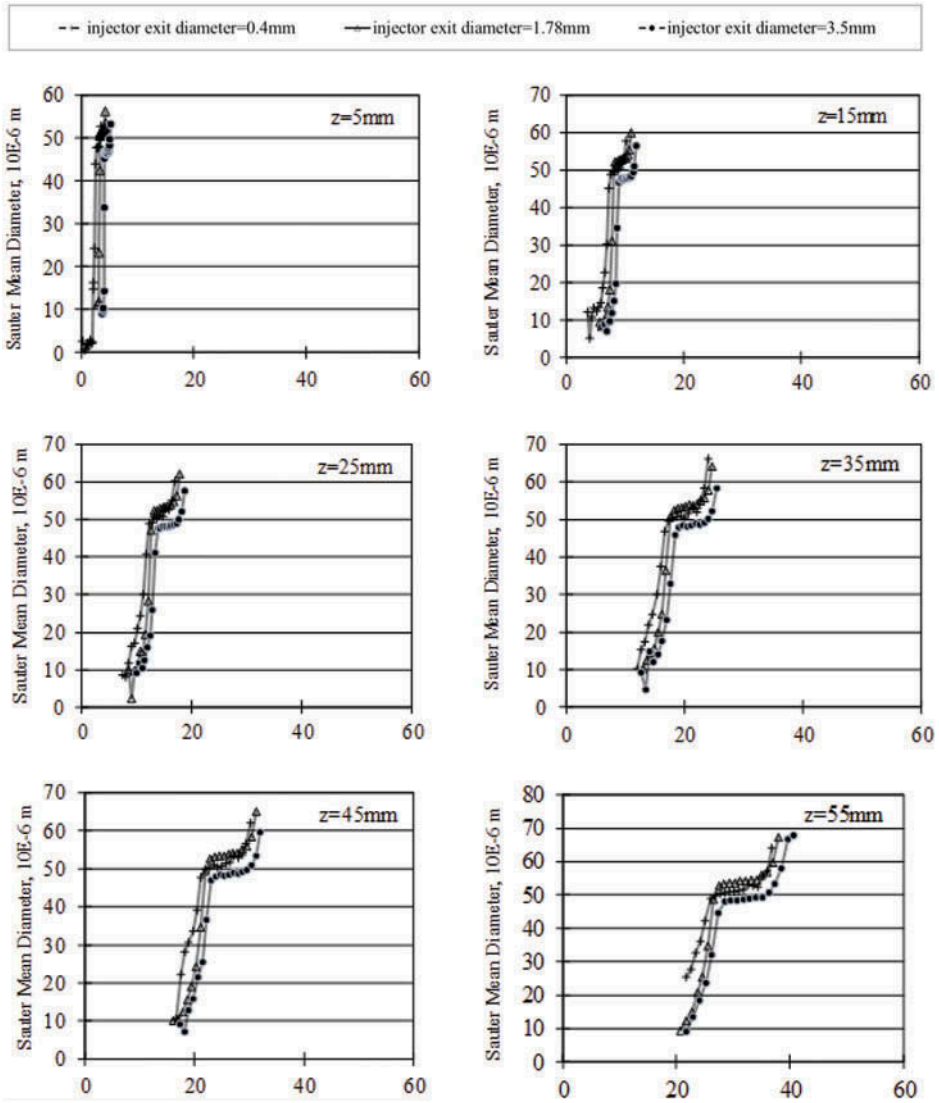

Figure 10 Predicted Sauter mean diameter at different heights with different injector exit diameters.

whereas on the right-hand side of the peak it is the region outside of the spray cone. With the injector exit diameter of 0.4 mm, the evaporated fuel gas inside the spray cone does not lead to immediate combustion but creates a rich fuel gas environment with a relatively low temperature profile as shown in Figure 11. Since the evaporation rate of droplets is related

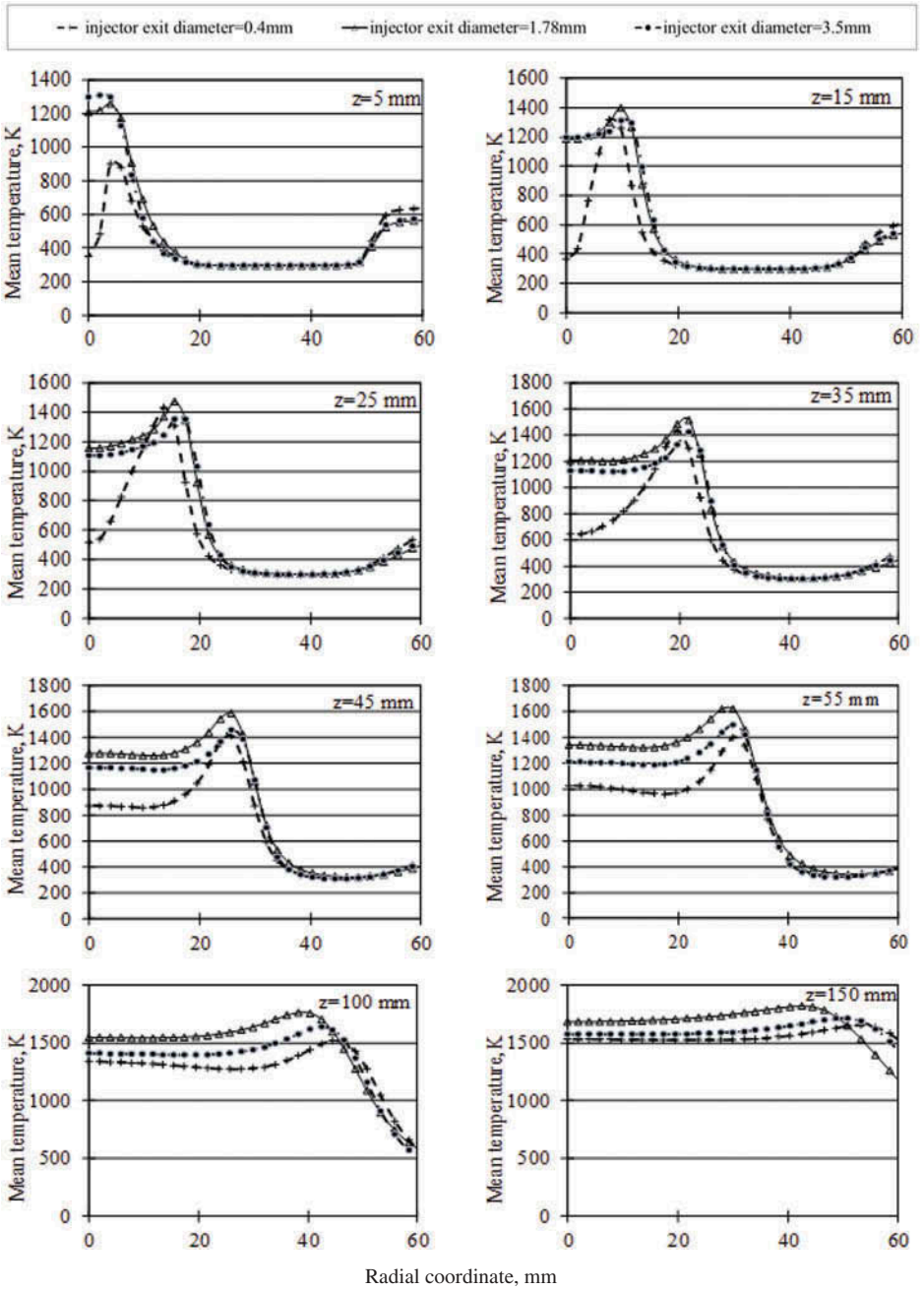

Figure 11 Predicted mean temperature profiles at different heights with different injector exit diameters.

to the surrounding fuel concentration, it slows down inside the spray cone and, therefore, the droplet number density at heights $z = 25$ mm, $z = 35$ mm, and $z = 45$ mm increases again above the level observed for the other investigated cases. The corresponding temperature grows with the height indicating that the fuel is consumed; after that the droplet number density decreases quickly to the same level as in the other cases. Outside of the spray cone (right side of the peak in droplet number density), the droplet number density with the injector exit diameter of 0.4 mm is, in general, lower than the other cases from height $z = 15$ mm, due to the consumption of evaporated fuel in the high temperature areas shown in Figure 11.

It is also observed in Figure 9 that, when the injector exit diameter increases from 0.4 mm to 1.78 mm or 3.5 mm, the radial locations of the peak in droplet number density increases correspondingly at low heights ($z = 5$ mm, 15 mm, and 25 mm). However, at higher elevations the peak in droplet number density in all cases appears at radial locations closer to each other, and almost at the same radial position at height $z = 55$ mm. This indicates that the spray trajectories are not following the original angle, but have been influenced by the air flow at high elevations. As a result, the analysis of the spray trajectory in the present study needs to be mainly based on the measured data at low heights.

With an injector exit diameter of 1.78 mm and 3.5 mm, the similar magnitude of droplet number density is observed at heights $z = 5$ mm, $z = 15$ mm, and $z = 25$ mm. Due to the larger injector exit diameter, the 3.5-mm case produces generally smaller droplets with the similar amount of droplets as in the 1.78-mm case (see Figure 10). However, at elevations $z = 35$–55 mm, there are more droplets that remained along the spray trajectory for the 3.5-mm case. At height $z = 5$ mm, combustion process is already visible, but the 3.5-mm case has a higher peak temperature than the 1.78-mm case, due to the less "rich fuel" environment inside spray cone. At higher elevations, the temperatures for the 3.5-mm case are, in general, lower than for the 1.78-mm case inside spray cone since less fuel exists in that region. In an outside spray cone both keep a similar profile till height $z = 100$ mm. Above this height, similar to the case with the injector exit diameter of 0.4 mm, the 3.5-mm case shows a higher temperature outside the spray cone. This indicates that when the injector exit diameter is 0.4 mm or 3.5 mm, the flame is wider than the 1.78-mm case. The origin of similarity in the flame behavior for the smallest and biggest injector exit diameter, as discussed above, is different.

With the same injector exit diameter of 1.78 mm but different dispersion angle of 6°, 10°, and 14°, the predicted droplet number density and SMD at various heights are shown in Figures 12 and 13, respectively. Figure 14 shows the corresponding temperature profiles. It can be noted that at $z = 5$ mm there is virtually the same distribution of the droplet sizes in all cases. The Sauter mean diameter in the region with high droplet number density (i.e., along the main trajectories) is similar at each height for all investigated cases. The main difference is that at higher elevations, wider distributions of droplets with a higher dispersion angle occur (see Figures 12 and 13).

According to Figure 14, at height $z = 5$ mm the peak temperature occurs inside the spray cone when the dispersion angle is 6° and 14° and along the spray trajectories for the remaining elevations. For the 10° case it occurs along the spray trajectory at every height. The temperature inside the spray cone decreases then for the 6° and 14° angles at height $z =$ 15 mm. Since then, the 6° case shows a similar temperature profile inside the spray cone as the 10°, while along the spray trajectory the peak temperature is lower. Temperature inside the cone in the 14° case at height $z = 15$ mm is still slightly higher than in the 10° case, but

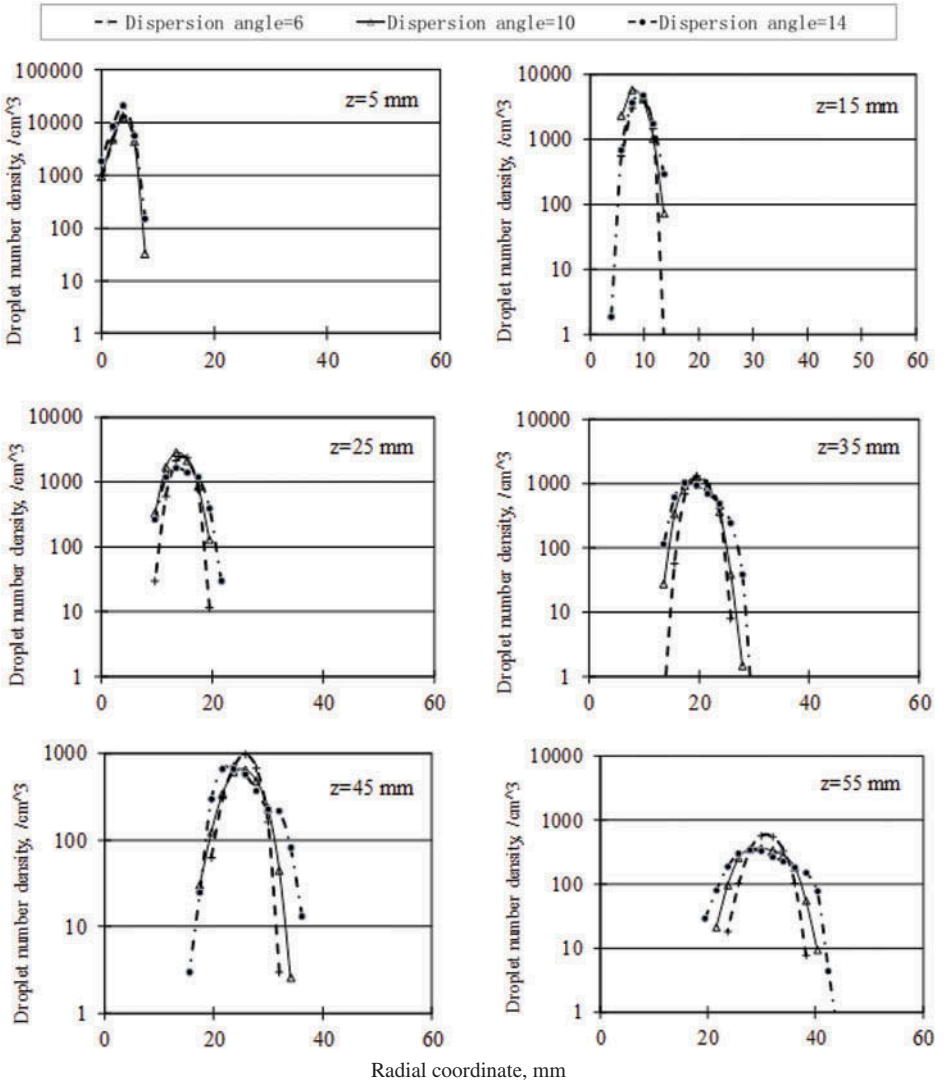

Figure 12 Predicted droplet number density at different heights with different dispersion angles.

it decreases further at height $z = 25$ mm, and it keeps this trend. Outside the spray cone, temperature in all cases has a similar profile below height $z = 55$ mm. Then the divergence between profiles is more pronounced due to the difference in the remaining amount of fuel. At height $z = 150$ mm it can be noted that for both the 6° and 14° case more fuel remained to be combusted leading to a higher temperature outside the spray cone than in the 10° case.

As a result, both the injector exit diameter and the dispersion angle have a considerable effect on the predictions. According to the analysis of the spray trajectory and distribution of droplet sizes and locations in the present study, the injector exit diameter of 1.78 mm and dispersion angle of 10° are used. This combination gives an acceptable agreement with the measured data as discussed below.

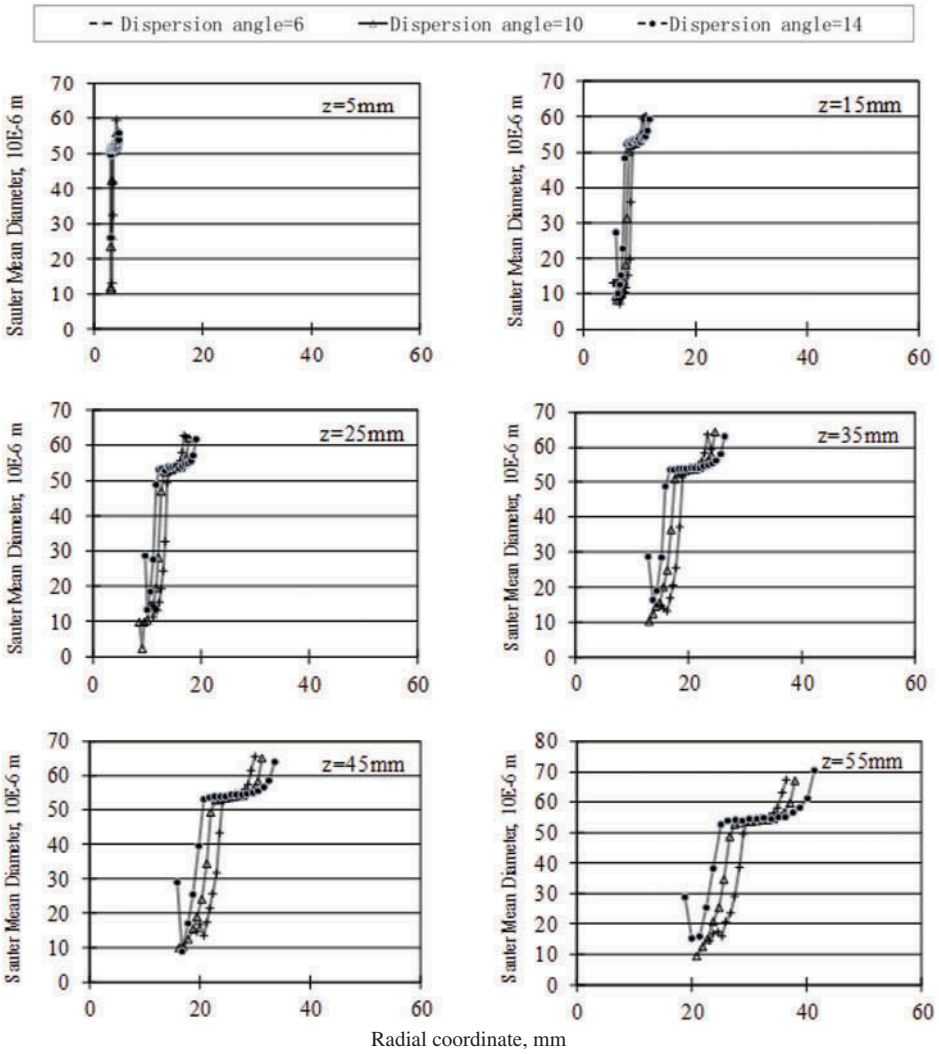

Figure 13 Predicted Sauter mean diameter at different heights with different dispersion angles.

Figure 15 shows the predicted SMD of the droplets in comparison with results of Crocker et al. (2001) and experimental data. In view of the uncertainties related to measurements and calculations of the SMD from captured droplets, the results obtained in the present study are very satisfactory. It is observed that at height $z = 5$ mm the SMD has higher deviations than at other heights. That might be because in the simulation at the nozzle exit the spray is directed towards the symmetry axis. In a 2D simulation all droplets then travel through the axis and the coalescence is overestimated according to the algorithm of O'Rourke (1981) and causes the droplet diameters to be more narrowly distributed. It has to be noted that the simulation does not predict any SMD in the inner region of the cone because no droplets reach that region, and this is in contrast with the experiment. In the results of Crocker et al. (2001) shown in Figure 15a, because the droplets are injected at

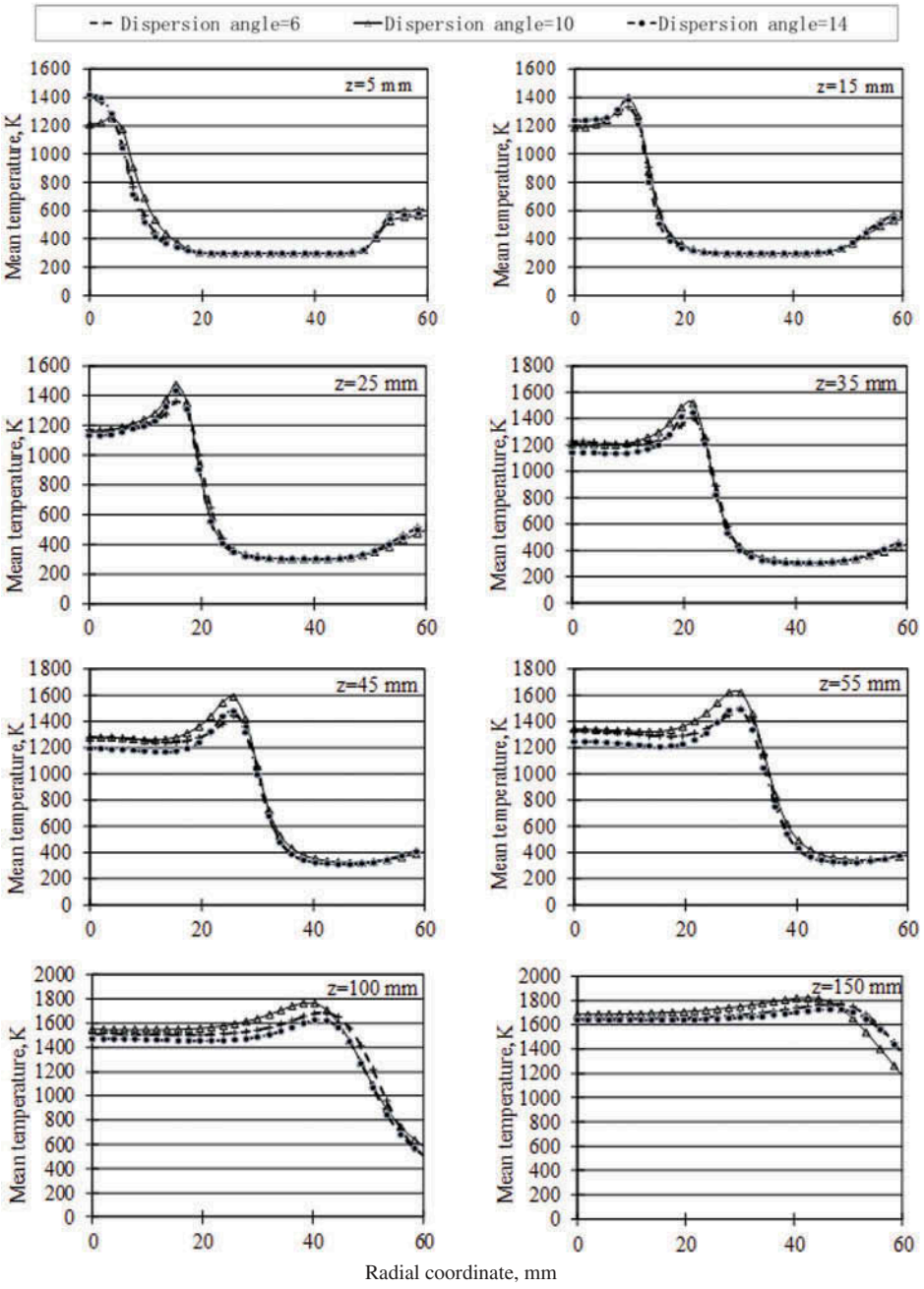

Figure 14 Predicted mean temperature profiles at different heights with different dispersion angles.

height $z = 5$ mm and the initial droplet size distribution at each radial position is taken directly from the measured data with 21,000 parcels of droplets, the predicted SMD shows better agreement with the experiment in regions with low droplet number density (aside of the main spray trajectory) than the present study. This behavior is visible especially at

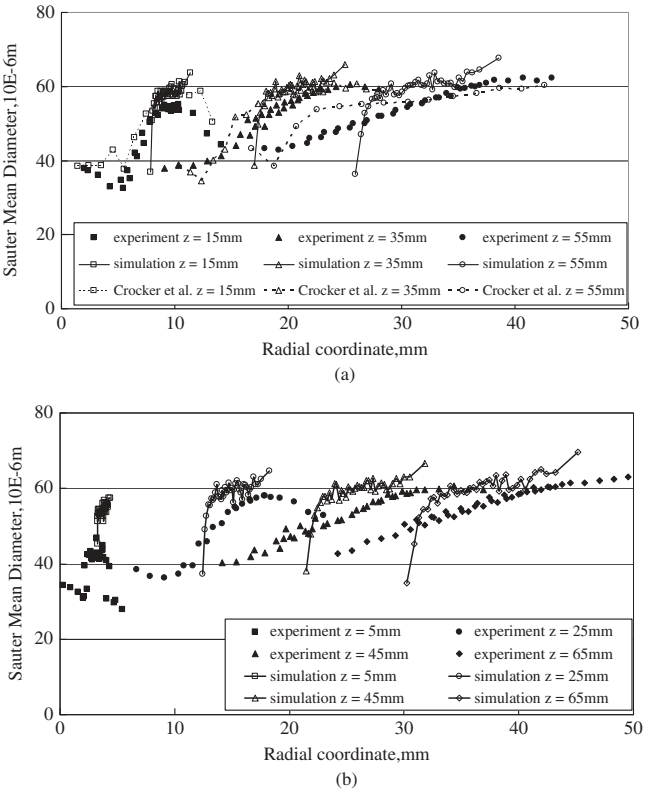

Figure 15 Predicted SMD of the droplets at different heights compared with results from Crocker et al. (2001) and the experiment.

height $z = 15$ mm. Large discrepancies between simulation of Crocker et al. (2001) and the experiment can be observed at further downstream positions. They proposed to use seven equally weighted parcels with a 1.5° interval centered on the mean angle, in order to fit the measured SMD. However, this action may also influence other predictions leading finally to significant discrepancy from the experiment.

The computed mean axial and radial velocities of the droplets are compared with results from Crocker et al. (2001) and with the experimental data in Figure 16. The predictions from the present study are in good agreement with the experiment in regions of significant importance, i.e., regions with high droplet number density (along the main spray trajectory) (see Figures 16a and 16b). In the region with low droplet number density, there are some discrepancies similar to those found in the comparison of the SMD. In the simulation of Crocker et al. (2001), the axial velocities are slightly underpredicted. Therefore, it was proposed to shift the initial droplet size to an even larger size. That would again lead to difficulties in other predictions.

In general, it is a feasible and effective approach to use the measured data of droplets, i.e., droplet size distribution and velocity components as the initial boundary condition of the spray. In this way, modeling of the primary breakup process, which is not well-understood, yet it can be avoided. Furthermore, since the data are usually measured at downstream positions, i.e., at least 5 mm away from the atomizer, the droplet coalescence,

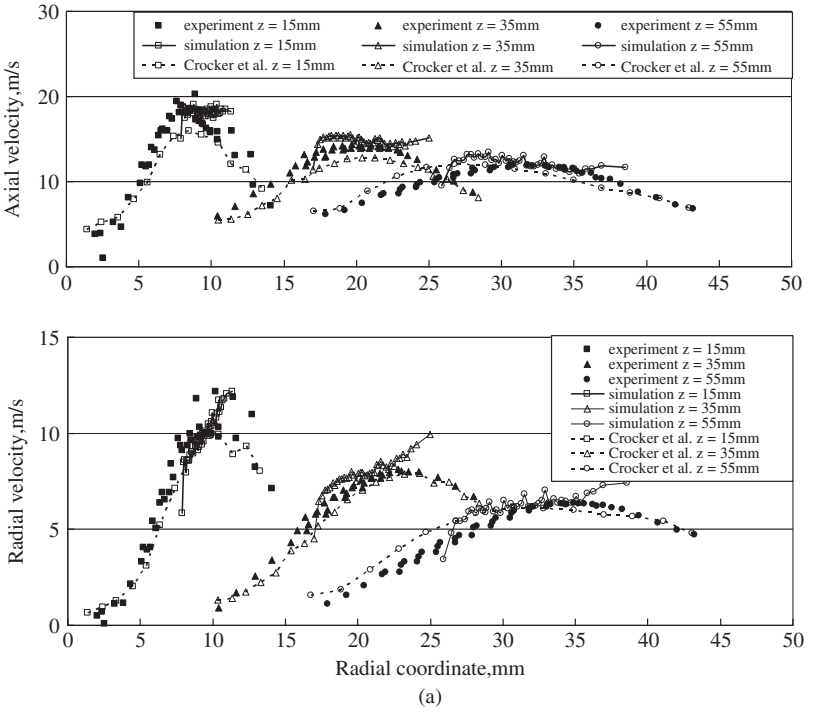

(a)

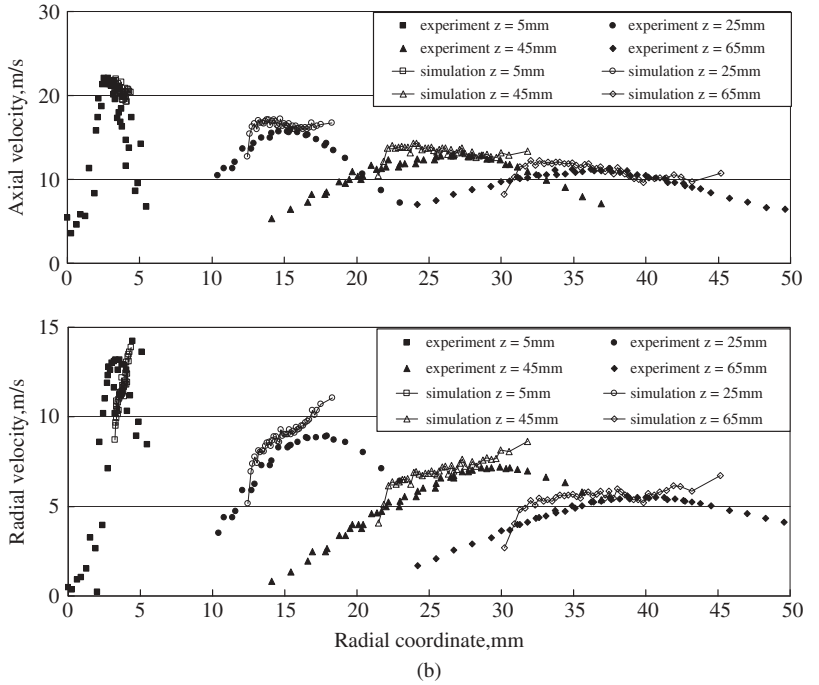

(b)

Figure 16 Predicted mean axial and radial velocities of the droplets at different heights compared with results from Crocker et al. (2001) and the experiment.

collision, and secondary breakup processes are mostly completed, and can be avoided in the simulation. As a result, the more accurate data we obtain in the experiment, the more accurate the description of the spray in the simulation is. However, as presented in the experiment of the NIST flame by Widmann and Presser (2002), the scattering of the droplets often leads to a very low measured spray flux close to the atomizer, i.e., about one-tenth of the total spray flux in the experiment of the NIST flame. Therefore, with the measured data of droplets, which is just a small part of the total injection, the accuracy of the boundary conditions is arguable and they still require further adjustments as done in the simulations of Crocker et al. (2001). It is possible to measure a larger fraction of the number of droplets at further downstream positions, but there it is more likely that the droplets have already interacted with the surroundings and they can hardly be used as boundary conditions. In some situations, i.e., with strong air flow, hot co-flow, or intense flame radiation, droplets may have been affected before they can be measured in the experiment. Besides, in order to guarantee an accurate description of the spray, a new set of measured data is required for the simulation when any change of the spray occurs, such as change of mass flow or pressure of the liquid fuel, effect of air flow, or radiation, etc., even when the same atomizer is used.

By contrast, in the present study the mass flow and pressure of the liquid fuel, spray angle, and dispersion angle are used to determine the droplet size distribution and velocity components, and this approach can be easily transferred to other conditions of research, especially for comparative study. One of the key points in this method is the analysis of the initial spray trajectory, which may differ with a different atomizer or liquid fuel. Unlike the other data, i.e., SMD or droplet velocity components, the spray trajectory can be analyzed in the experiment relatively easily, and can be analyzed even at closer positions to the atomizer in order to eliminate the influences of the surroundings. The obtained initial spray trajectory is usually accurate enough for simulations even if just a small proportion of droplets can be measured in the experiment. As shown above, in regions of high importance (regions with high droplet number density), the droplet number density, SMD, and the mean axial and radial velocities of the droplets predicted in current research have shown improved agreement with the experimental data in comparison to other studies. The disadvantage of the method used in the present study is that the models for droplet coalescence, collision, and secondary break-up require further improvements so that the droplets in regions with low number density can also be predicted correctly. Therefore, we suggest improving the collision and coalescence model by generating more widely distributed small droplets. The trajectory of the spray will not change by this modification and the predicted droplet velocity and SMD in regions with low droplet number density will match the experiment better.

Furthermore, temperature measurements in the flame are not present in the experimental study due to the large uncertainties associated with such measurements in spray flames. Only a temperature of about 550 K at the exit of the exhaust channel was indicated. However, in both simulations of Crocker et al. (2001) and the current study the exhaust channel is omitted. Therefore, the direct comparison is not possible. A peak temperature of about 1800 K is reported by Crocker et al. (2001), while in the present study the magnitude is approximately 50 K higher. In the current research the average temperature at the outlet location is equal to around 700 K. Since in the experiment the temperature was measured further downstream than in the numerical study, it is expected that a temperature of 700 K is a good approximation of the experimental conditions at the outlet.

In order to further validate the spray flame behavior, the definition of oxidation mixture ratio (Yang and Blasiak, 2005) is introduced:

$$R_O = \frac{m_O}{m_O + \sum_c S_c m_{F,c}} \tag{15}$$

where $S = n_o M_O / n_F M_F$ with m being the mass fraction, n the stoichiometric ratio, M the molar mass, and index O, F, and C representing oxygen, fuel, and flue gas, respectively. The lean flammability limit can be used to define the external boundary of the flame, and the rich flammability limit can be used to define the inner boundary of the flame. Following Yang and Blasiak (2005), we assumed that $R_O = 0.99$ is representative for the external boundary. From Figure 17 it can be noticed that contours of mean oxidation mixture ratio resemble the flame photographs in the experiment of Widmann and Presser (2002) well and it qualitatively confirms that the predicted mean concentration of OH is capable of representing the flame profile.

The influence of the source term of the mixture fraction variance because of evaporation on the NIST flame was investigated as well and presented in Zhu et al. (2011). Due to the evaporation of the droplets, the peak value of mean mixture fraction variance rises from 0.013 to 0.016. The main difference occurs at the root of the flame, where most of the evaporation takes place. This is also the same region where the scalar dissipation changes with the peak value of scalar dissipation increasing from $13s^{-1}$ to $17s^{-1}$. Since in the NIST flame the influence of the source term on the mixture fraction variance only occurs in this lower region while the combustion mainly occurs in the flame area, the combustion characteristics are not strongly influenced by the modeling of the variance equation.

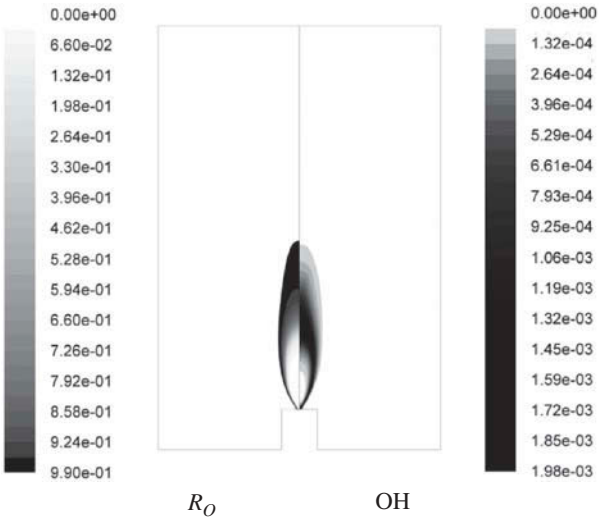

Figure 17 Predicted contours of mean oxidation mixture ratio, R_O and mean mole fraction of OH.

CONCLUSIONS

We have presented results of a numerical investigation of a methanol spray flame studied experimentally at the NIST by Widmann and Presser (2002). We also have analyzed previous simulations of this flame performed by Crocker et al. (2001), De Jager (2008), and Collazo et al. (2009).

In spite of the asymmetric position of the exhaust channel, the flame can be considered to be statistically symmetric. Therefore, in the employed RANS approach the computational domain can be taken as two dimensional, allowing for a sufficiently fine grid, especially in the near nozzle region where large velocity and temperature gradients are present.

Based on the analysis of $y+$ value in the near-wall region we used the enhanced wall treatment instead of the wall function used in previous simulations, e.g., by De Jager (2008) in the frame of the standard k-ε model. The choice of model for the near wall region provided better predictions of the velocity components of the gaseous phase at various downstream positions. The observed deviations between model predictions and experimental results at small radial distance may be attributed to both numerical and experimental causes, and have been observed also in previous simulations by others, see Crocker et al. (2001) and De Jager (2008).

In order to take into account droplet collision, coalescence, and secondary breakup, the Eulerian–Lagrangian method was used with the LISA model for the atomization process. The measured data were analyzed in order to obtain relative accurate boundary conditions of the spray, which is especially of high importance to the injector exit diameter (see Eq. (1)) for the analysis of the initial spray trajectory. This method was compared and discussed with the approach used in Crocker et al. (2001), in which the measured data of droplets were used as the boundary conditions of the spray. Since often a very low spray flux can be measured close to the atomizer in the experiment and the droplets may have interacted with the surroundings if they are measured further downstream, the measured data of droplets, i.e., droplet size distribution and velocity components, still require adjustments before they can be used. Also, when we use the measured data as boundary conditions of the spray, it is necessary to measure a new set of data if any change of the atomizer or process conditions is made. This limits the transferability of the models. In the method used in the present study, the required analysis of the initial spray trajectory needed to define the boundary conditions of the spray can be made relatively easy and the spray model can be easily transferred to other conditions, especially for comparative investigations. In regions of major importance with high droplet number density, the predictions of droplet number density, SMD, and the mean axial and radial velocities of the droplets showed improved match with the experimental data with regard to results of previous investigations. Nevertheless, it is found that models for droplet coalescence, collision, and secondary break-up processes require further improvements so that the droplets in regions with low number density can also be predicted with higher precision, and we suggest to improve the collision and coalescence model by generating more widely distributed small droplets.

Additionally, the effects of influential parameters in the spray model, such as injector exit diameter and dispersion angle, on the predictions are investigated. Different parameters lead to different profiles of droplet number density, Sauter mean diameter, and temperature. Therefore, it is crucial to use boundary conditions adequate to the settings of the experiment.

The introduction of the steady flamelet model with a detailed reaction mechanism for gaseous combustion, and the discrete ordinates model for radiation also contributes to the good agreement between the predictions and the experimental data. Unfortunately, temperature and species measurements in the flame zone are not available in the experiment for validation. It is found that contours of mean OH concentration and mean oxidation mixture ratio both resemble well the flame photographs in the experiment of Widmann and Presser (2002), and a predicted temperature of 700 K at the outlet in the simulation is a good approximation of the experimental conditions at the exit. The investigation of the influence of the source term of evaporation on the mean mixture fraction variance has shown that, due to the evaporation process, the peak value of mean mixture fraction variance increased from 0.013 to 0.016. However, the change only occurred in the root part of the flame and not in the main flame area, so the combustion characteristics do not change much.

ACKNOWLEDGMENT

The authors would like to thank C. Presser for the NIST database.

FUNDING

The Technology Foundation STW is gratefully acknowledged for financial support.

REFERENCES

Binniger, B., Chan, M., Paczkko, G., and Herrmann, M. 1998. Numerical simulation of turbulent partially premixed hydrogen flames with the flamelet model. Technical Report. Advanced Combustion Gmbh, Internal Report.

Collazo J., Porteiro, J., Patiño, D., Miguez, J.L., Granada, E. and Moran, J. 2009. Simulation and experimental validation of a methanol burner. *Fuel*, **88**, 326–334.

Crocker, D.S., Widmann, J.F., and Presser, C. 2001. CFD modeling and comparison with data from the NIST reference spray combustor. Presented at the ASME International Mechanical Engineering Congress and Exposition, New York, November 11–16.

De Jager, B. 2008. Combustion and noise phenomena in turbulent alkane flames. PhD thesis. Twente University, the Netherlands.

Dombrowski, N., and Hooper, P.C. 1962. The effect of ambient density or drop formation in sprays. *Chem. Eng. Sci*., **17**, 291–305.

Düwel, I., Ge, H.-W., Kronemayer, H., Dibble, R., Gutheil, E., Schulz, C., and Wolfrum, J. 2007. Experimental and numerical characterization of a turbulent spray flame. *Proc. Combust. Inst*., **31**, 2247–2255.

Han, Z., Perrish, S., Farrell, P.V., and Reitz, R.D. 1997. Modeling atomization processes of pressure-swirl hollow-cone fuel sprays. *Atomization Sprays*, **7**, 663–684.

Hollmann, C., and Gutheil, E. 1996. Modeling of turbulent spray diffusion flames including detailed chemistry. *Symp. (Int.) Combust*., **26**, 1731–1738.

Jenny, P., Roekaerts, D., and Beishuizen, N. 2012. Modeling of turbulent dilute spray combustion. *Prog. Energy Combust. Sci*., **38**, 846–887.

Kader, B. 1981. Temperature and concentration profiles in fully turbulent boundary layers. *Int. J. Heat Mass Transfer*, **24**, 1541–1544

Karpetis, A., and Gomez, A. 2000. An experimental study of well-defined turbulent nonpremixed spray flames. *Combust. Flame*, **121**, 1–23.

Lefebvre, A.H. 1989. *Atomization and Sprays*. Hemisphere Publishing Corporation, New York.

Lindstedt, P., and Chen, J.Y. 2010. International workshop on measurement and computation of turbulent nonpremixed flames. Available at: http://www.sandia.gov/TNF/chemistry.html.

Lindstedt, R.P., and Meyer, M.P. 2002. A dimensionally reduced reaction mechanism for methanol oxidation. *Proc. Combust. Inst*., **29**, 1395–1402.

Magnussen, B.F. 1981. On the structure of turbulence and a generalized eddy dissipation concept for chemical reaction in turbulent flow. In *Proceedings of the 19th AIAA Meeting*, St. Louis, MO, January 12–15.

McDonell, V.G., and Samuelsen, G.S. 1995. An experimental database for the computational fluid dynamics of reacting and nonreacting methanol sprays. *J. Fluids Eng*., **117**, 145–153.

Muller, C.M., Breitbach, H., and Peters, N. 1994. Partially premixed turbulent flame propagation in jet flames. *Symp. (Int.) Combust*., **25**(1), 1099–1106.

NIST. 2010. Materials measurement laboratory. Gaithersburg, Maryland. U. Benchmark spray combustion database. Available at: http://webbook.nist.gov/chemistry/spray-combust.

O'Rourke, P.J. 1981. Collective drop effects on vaporizing liquid sprays. PhD thesis, Princeton University, Princeton, New Jersey.

O'Rourke, P.J., and Amsden, A.A. 1987. The TAB method for numerical calculation of spray droplet breakup. SAE Paper 872089.

Patterson, M.A., and Reitz, R.D. 1998. Modeling the effects of fuel spray characteristics on diesel engine combustion and emission. SAE Paper 980131.

Presser, C. 2006. Application of a benchmark experimental database for multiphase combustion modelling. *J. Propuls. Power*, **22**, 1145–1148.

Ranz, W.E., and Marshall, Jr., W.R. 1952a. Evaporation from drops, Part I. *Chem. Eng. Prog*., **48**, 141–146.

Ranz, W.E., and Marshall, Jr., W.R. 1952b. Evaporation from drops, Part II. *Chem. Eng. Prog*., **48**, 173–180.

Reitz, R.D. 1987. Modeling atomization processes in high-pressure vaporizing sprays. *Atomization Sprays*, **3**, 309–337.

Schmidt, D.P., Corradini, M.L., and Rutland, C.J. 1999a. A two-dimensional, non-equilibrium model of flashing nozzle flow. In *Proceedings of the 3rd ASME/JSME Joint Fluids Engineering Conference*, San Francisco, July 18–23; ASME, New York.

Schmidt, D.P., Nouar, I., Senecal, P.K., Rutland, C.J., Martin, J.K., and Reitz, R.D. 1999b. Pressure-swirl atomization in the near field. SAE Technical Paper 1999-01-0496.

Taylor, G.I. 1963. The shape and acceleration of a drop in a high speed air stream. Technical Report. In the Scientific Papers of G. I. Taylor, ed., G. K. Batchelor.

Weber, C. 1931. Zum Zerfall eines Flüssigkeitsstrahles. *ZAMM*, **11**, 136–154.

Widmann, J.F., and Presser, C. 2002. A benchmark experimental database for multiphase combustion model input and validation. *Combust Flame*, **129**, 47–86.

Yang, W., and Blasiak, W. 2005. Numerical study of fuel temperature influence on single gas jet combustion in highly preheated and oxygen deficient air. *Energy*, **30**, 385–398.

Zhu, S., Roekaerts, D., and van der Meer, T. 2011. Numerical simulation of a turbulent methanol spray flame using the Eulerian–Lagrangian method and the steady laminar flamelet model. In *Proceedings of the 7th Mediterranean Combustion Symposium*, Sardinia, Italy, September 11–15; ID: PEC-4.